Cellular/Molecular

Low-Threshold Ca^{2+} Current Amplifies Distal Dendritic Signaling in Thalamic Reticular Neurons

Shane R. Crandall,[3,4] G. Govindaiah,[2,4] and Charles L. Cox[1,2,3,4]

Departments of [1]Pharmacology and [2]Molecular and Integrative Physiology, [3]Program in Neuroscience, and [4]Beckman Institute for Advanced Science and Technology, University of Illinois, Urbana, Illinois 61801

The low-threshold transient calcium current (I_T) plays a critical role in modulating the firing behavior of thalamic neurons; however, the role of I_T in the integration of afferent information within the thalamus is virtually unknown. We have used two-photon laser scanning microscopy coupled with whole-cell recordings to examine calcium dynamics in the neurons of the strategically located thalamic reticular nucleus (TRN). We now report that a single somatic burst discharge evokes large-magnitude calcium responses, via I_T, in distal TRN dendrites. The magnitude of the burst-evoked calcium response was larger than those observed in thalamocortical projection neurons under the same conditions. We also demonstrate that direct stimulation of distal TRN dendrites, via focal glutamate application and synaptic activation, can locally activate distal I_T, producing a large distal calcium response independent of the soma/proximal dendrites. These findings strongly suggest that distally located I_T may function to amplify afferent inputs. Boosting the magnitude ensures integration at the somatic level by compensating for attenuation that would normally occur attributable to passive cable properties. Considering the functional architecture of the TRN, elongated nature of their dendrites, and robust dendritic signaling, these distal dendrites could serve as sites of intense intra-modal/cross-modal integration and/or top-down modulation, leading to focused thalamocortical communication.

Introduction

The GABAergic thalamic reticular nucleus (TRN) plays a central role in modulating information transfer between thalamus and neocortex, as well as within the thalamus (Yingling and Skinner, 1976; Crick, 1984; Steriade et al., 1986, 1993; Crabtree et al., 1998; Crabtree and Isaac, 2002). Centrally located in the thalamocortical circuit, corticothalamic and thalamocortical axons pass through the TRN, providing the primary sources of synaptic inputs to the nucleus (Jones, 1975; Ohara and Lieberman, 1981; Liu and Jones, 1999; Guillery and Harting, 2003). In turn, TRN axons project into the thalamus in which they modify thalamic activities such as neuronal excitability (Cox et al., 1997; Kim et al., 1997) and receptive field properties (Lee et al., 1994a,b). Thus, the TRN is ideally located for modulating thalamocortical communication via neocortical-driven feedforward or thalamic-driven feedback inhibition.

Ultimately, the magnitude of inhibition onto the dorsal thalamus depends critically on the voltage state of the TRN neuron. Like most thalamic neurons, TRN neurons respond to excitatory input by discharging Na^+-dependent action potentials (APs) in one of two distinct modes: tonic or burst (Llinás and Jahnsen, 1982; Spreafico et al., 1988; Avanzini et al., 1989; Contreras et al., 1993). Transitioning between burst and tonic mode depends on the presence of the low-threshold transient calcium (Ca^{2+}) current, I_T, which is inactivated at relatively depolarized membrane potentials and deinactivated at relatively hyperpolarized membrane potentials (Huguenard and Prince, 1992; Huguenard, 1996). In the deinactivated state, sufficient excitatory input can activate I_T, resulting in a large Ca^{2+} depolarization known as a low-threshold spike (LTS), which in turn generates a high-frequency burst discharge of Na^+-dependent action potentials.

Despite understanding the role of I_T in generating burst output, how this current is distributed across the neuron and more importantly how it contributes to the integration of afferent information remains speculative. Previous studies have suggested a dendritic distribution of I_T in TRN neurons, but these studies have been limited because of technical considerations (Destexhe et al., 1996; Joksovic et al., 2005; Cueni et al., 2008; Kovács et al., 2010). Although this issue has been explored in thalamocortical relay neurons in which there appears to be a heterogeneous distribution of I_T (Munsch et al., 1997; Zhou et al., 1997; Destexhe et al., 1998; Williams and Stuart, 2000), any comparison between TRN and thalamocortical neurons is difficult because of their distinct morphologies and burst properties (Huguenard and Prince, 1992).

In this study, we used two-photon laser scanning microscopy (2PLSM) coupled with whole-cell patch recordings to characterize the somatodendritic distribution of I_T along individual TRN dendrites. Here we show that a somatic burst discharge produces a transient Ca^{2+} current along the entire length of TRN dendrites, which increases in magnitude at greater distances from the soma. Importantly, we also show that the direct stimulation of

Received July 13, 2010; revised Aug. 30, 2010; accepted Sept. 13, 2010.

This work was supported by the National Institutes of Health/National Eye Institute (C.L.C.) and a National Institute on Deafness and Other Communication Disorders training grant (S.R.C.). We thank Drs. Yanyan Wang and Kush Paul for helpful comments on this manuscript.

Correspondence should be addressed to Charles L. Cox, 2357 Beckman Institute, 405 North Mathews Avenue, Urbana, IL 61801. E-mail: cox2@illinois.edu.

DOI:10.1523/JNEUROSCI.3636-10.2010

 0270-6474/10/3015419-11$15.00/0

individual distal dendrites can locally activate distal I_T, leading to the amplification of afferent input. These finding have important implications for understanding how TRN neurons modulate thalamic transmission, as well as thalamocortical operations.

Materials and Methods

Slice preparation. Thalamic slices were prepared from young Sprague Dawley rats (postnatal age, 11–23 d) of either sex by using published procedures with minor modifications (Govindaiah and Cox, 2004). Briefly, rats were anesthetized with pentobarbital sodium (50 mg/kg) and perfused with cold oxygenated slicing solution before being decapitated. Brains were quickly removed and placed in cold (4°C) oxygenated (5% CO_2, 95% O_2) slicing solution containing the following (in mM): 2.5 KCl, 1.25 NaH_2PO_4, 10.0 $MgSO_4$, 0.5 $CaCl_2$, 26.0 $NaHCO_3$, 10.0 glucose, and 234.0 sucrose. Thalamic slices (250–300 μm) were cut in the horizontal plane for TRN/ventrobasal (VB) nucleus recordings or the coronal plane for dorsal lateral geniculate nucleus (dLGN) recordings. Slices were immediately transferred to a holding chamber with oxygenated physiological saline (31 ± 1°C) containing the following (in mM): 126.0 NaCl, 2.5 KCl, 1.25 NaH_2PO_4, 2.0 $MgCl_2$, 2.0 $CaCl_2$, 26.0 $NaHCO_3$, and 10.0 glucose. After 15–20 min, the holding chamber was reduced to room temperature, and slices were further incubated for a minimum of 60 min before recording.

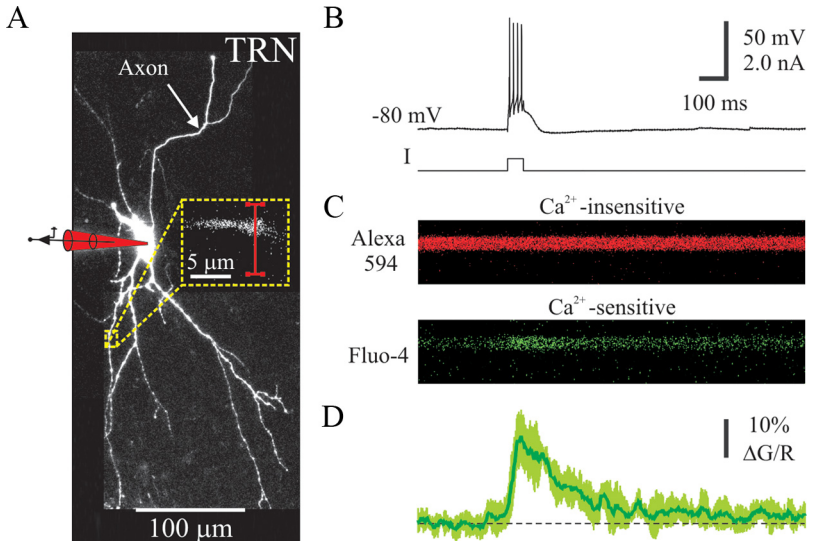

Figure 1. Measurement of dendritic Ca^{2+} responses evoked by somatic burst discharge in TRN neurons. ***A***, Stacked 2PLSM image of a TRN neuron filled. The yellow box indicates the dendritic region from which a line scan was performed (75 μm). ***B***, Somatic recording of a burst discharge elicited from a hyperpolarized holding potential by injecting a short depolarizing current pulse. ***C***, Simultaneous line scan of both the calcium-insensitive (Alexa Fluor 594, red) and calcium-sensitive (Fluo-4, green) fluorescent signals. ***D***, The average $\Delta G/R$ response obtained from the dendritic region shown in ***A***. The average (dark green line) and SD (light green envelope) were obtained from five consecutive burst discharges.

Whole-cell recording procedures. For recording, individual slices were transferred to a recording chamber that was maintained at room temperature (23 ± 2°C) with oxygenated physiological saline (2.5–3 ml/min). Individual neurons were identified using Dodt contrast optics, and whole-cell recordings were obtained using recording pipettes containing the following (in mM): 117 K-methylsulfonate, 13 KCl, 2.0 $MgCl_2$, 10.0 HEPES, 2.0 Na_2-ATP, and 0.4 Na-GTP, pH 7.3 (290 mOsm). Pipettes also contained a Ca^{2+}-sensitive indicator (Fluo-4, 125 μM) and a Ca^{2+}-insensitive indicator (Alexa Fluor 594, 25 μM). The dual indicators allowed for visualization of small distal dendrites and provided a substantially less noisy measurement of Ca^{2+} changes than the use of a single indicator (Yasuda et al., 2004). The final pipette solution resulted in a junction potential of ~10 mV and was corrected for in all voltage recordings. During recordings, pipette capacitance was neutralized, and the access resistance was continually monitored.

Pharmacological agents were prepared and stored as recommended and diluted in physiological saline to a final concentration before use. All antagonists were bath applied 10–15 min before subsequent experimental tests. Tetrodotoxin (TTX), ω-conotoxin-MVIIC, 3-((*R*)-2-carboxypiperazin-4-yl)-propyl-1-phosphonic acid (CPP), 6, 7-dinitroquinoxaline-2,3-dione (DNQX), and mibefradil were all purchased from Tocris Bioscience, and all other compounds were from Sigma.

Stimulation of distal dendrites was accomplished by local glutamate application or electrical stimulation. Focal glutamate application was achieved by pressure ejection (0.5–1 mM, 0.75–3 psi, 30–50 ms duration) via a glass pipette (1–3 μm tip diameter). Pipettes also contained Alexa Fluor 594 (12.5 μM), to aid in locating, positioning, and visualizing the ejection site. Only focal ejections with a minimal radial spread (<25 μm) were used for analysis. Line scans were performed at the edge of the stimulated area to limit the amount of dendritic movement caused by pressure ejection. Synaptic stimulation was achieved by placing a bipolar electrode adjacent to TRN within the internal capsule (single stimulus: 40–300 μA, 500 μs duration, 0.1 Hz).

Calcium imaging and analysis. Ca^{2+} imaging was performed simultaneously with whole-cell recordings using a custom two-photon laser scanning microscope (Ultima; Prairie Technologies) coupled with a titanium:sapphire laser (MaiTai HP; Spectra Physics). Imaging was accomplished by laser excitation (820 nm) via a high numerical aperture water-immersion objective (60×; Olympus). To allow sufficient filling of dendritic arbor with fluorescent indicators, imaging was initiated 20–30 min after obtaining whole-cell configuration. Once a location was selected for imaging, the fluorescence was averaged over the spatial extent of the structure using line scans (15–20× optical zoom) with a temporal resolution of ~2.5 ms. On average, five line scans were collected at each location with 10–15 s intervals between scans.

Image acquisition was performed using custom Prairie View Software and analyzed *post hoc* using NIH ImageJ software. The reported change in fluorescence ($\Delta G/R$) was calculated as the change in fluorescence from baseline of the Ca^{2+}-sensitive indicator (Fluo-4) normalized to the average fluorescence of the Ca^{2+}-insensitive indicator (Alexa Fluor 594): $\Delta G/r = (G_{Peak} - G_o)/R_{Avg}$ (Sabatini et al., 2002). Baseline fluorescence (G_o) was calculated as the average fluorescence of the 200 ms before the stimulus. The peak response was calculated as the combined average of each line scan smoothed with a ~30 ms running average. Physiological recordings were analyzed using pClamp software (Molecular Devices). Population data are expressed as mean ± SD, and significance was defined as $p < 0.05$. A paired *t* test was used for analyses unless otherwise indicated.

Results

Combining whole-cell electrophysiological recordings with 2PLSM, we initially measured dendritic Ca^{2+} changes in response to a somatic burst discharge in TRN neurons. Individual neurons were loaded via patch pipette with a Ca^{2+}-insensitive indicator (Alexa Fluor 594, 25 μM) to facilitate the localization of small dendrites and a Ca^{2+}-sensitive indicator (Fluo-4, 125 μM) to monitor Ca^{2+} changes (Fig. 1*A*). A single burst discharge was evoked by somatic current injection (25–75 ms; 100–400 pA), whereas the initial membrane potential at the soma was held between −80 and −90 mV (Fig. 1*B*). The resulting change in Ca^{2+} was monitored simultaneously using a high-resolution line scan and quantified as the change in green fluorescence normalized to the average red fluorescence ($\Delta G/R$) (Fig. 1*C*,*D*). Although nonbursting neurons have been reported within the TRN (Contreras et al., 1992; Brunton and Charpak, 1997; Lee et al.,

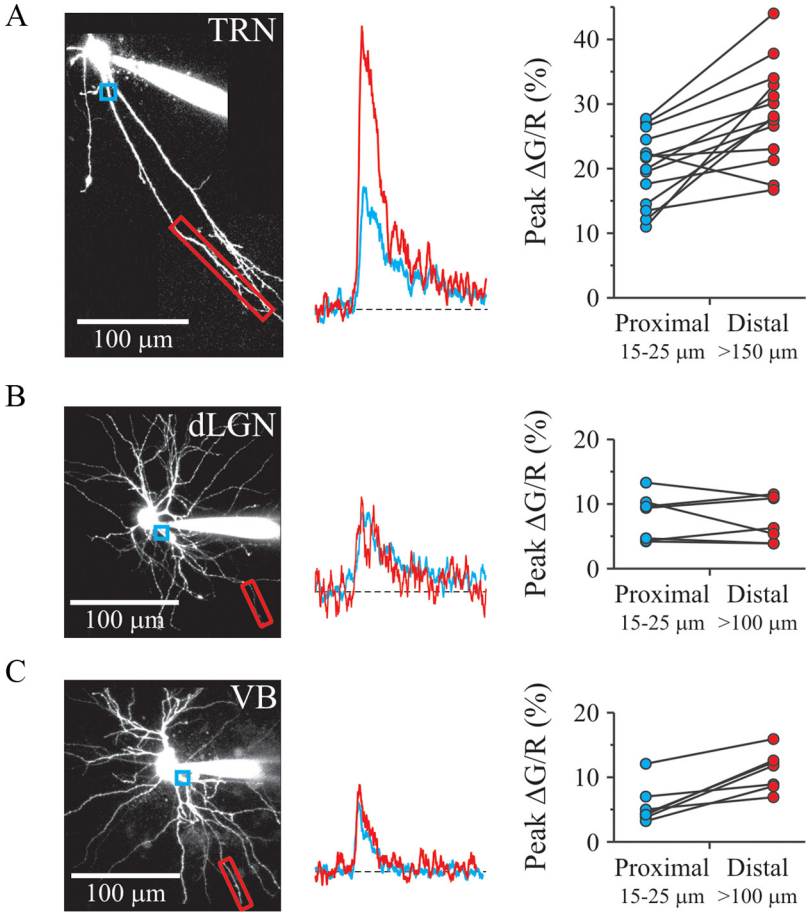

Figure 2. Burst discharge produces a robust Ca^{2+} response in distal dendrites of TRN neurons. ***A***, Left, Stacked 2PLSM image of an example TRN neuron filled. The blue box indicates the dendritic region from which a proximal line scan was typically obtained (15–25 μm). The red box indicates the dendritic region from which a distal line scan was typically obtained (>150 μm). Middle, Proximal (blue) and distal (red) Ca^{2+} responses obtained from a different TRN neuron. Right, Population data collected from 14 dendrites. ***B***, Left, Stacked 2PLSM image of an example dLGN neuron filled. Blue box indicates dendritic region from which a proximal line scan was typically obtained (15–25 μm). The red box indicates the dendritic region from which a distal line scan was typically obtained (>100 μm). Middle, Proximal (blue) and distal (red) Ca^{2+} responses obtained from a different dLGN neuron. Right, Population data collected from seven dendrites. ***C***, Left, Stacked 2PLSM image of an example VB neuron filled. Boxes represent the same region as in ***B***. Middle, Proximal (blue) and distal (red) Ca^{2+} responses obtained from a different VB neuron. Right, Population data collected from seven dendrites.

2007), in this study, all recordings were obtained from neurons that produced burst discharge.

Burst discharge evokes a robust distal Ca^{2+} response

Consistent with a previous report (Cueni et al., 2008), somatic burst discharge in TRN neurons reliably produced a dendritic Ca^{2+} response. To determine whether the magnitude of the response was dependent on dendritic location, we initially compared proximal and distal Ca^{2+} responses obtained from the same dendrite (Fig. 2*A*). In 13 of 14 TRN dendrites examined (93%), a somatic burst discharge produced a larger Ca^{2+} response at the distal location (>150 μm) when compared with the proximal location (15–25 μm) [proximal, 20.0 ± 5.6%; distal, 28.5 ± 7.5%; n = 14 dendrites (D)/12 neurons (N); $p < 0.001$, paired t test]. There were only two instances in which two dendrites were sampled from the same neuron. In both cases, the pair of dendrites displayed a comparable proximal–distal increase. On average, the distal location had a 143% larger response than the proximal location. To determine whether the magnitude of the Ca^{2+} response observed in TRN neurons was common to other bursting thalamic cell types, we performed the same experiment on thalamocortical projection neurons of the dLGN and VB nucleus (Fig. 2*B*,*C*). For dLGN dendrites, no significant difference was observed between distal (>100 μm) and proximal Ca^{2+} responses (proximal, 8.0 ± 3.6%; distal, 7.6 ± 3.5%; n = 7D/5N; $p = 0.69$, paired t test). In contrast, VB dendrites did generate a larger distal Ca^{2+} response (proximal, 5.7 ± 3.1%; distal, 11.0 ± 3.0%; n = 7D/4N; $p < 0.01$, paired t test). Although a single burst discharge produced a dendritic Ca^{2+} response in all three thalamic cell types examined, the magnitude of the TRN responses was considerably larger than those of thalamocortical projection neurons.

To further characterize the dendritic/Ca^{2+} relationship in TRN neurons, we proceeded to image 22 new dendrites, but this time, we performed multiple line scans (four to six) along the somatodendritic axis at ~50 μm intervals (Fig. 3*A*,*B*). Of the dendrites examined, 19 (86%) displayed a positive dendritic slope or an increased Ca^{2+} response with a greater measured distance from soma. In general, TRN dendrites displayed a range of slopes with an average increase of 0.05% $\Delta G/R$ per micrometer (maximum, 0.14%/μm; minimum, −0.06%/μm). For most dendrites (68%), the largest Ca^{2+} response was at a distance >100 μm from soma; however, in a small population of dendrites, the largest response occurred between 50 and 75 μm (27%). Despite some variability, the vast majority of TRN dendrites did display an increasing proximal-to-distal gradient, further supporting the hypothesis that distal locations have larger Ca^{2+} signals.

Considering the relationship between the Ca^{2+} amplitude and dendritic distance ($r = 0.34$, $p < 0.01$, Pearson's correlation; data not shown), could a change in dendritic diameter account for the change in magnitude? In layer V pyramidal neurons, it has been shown that differences in dendritic diameter (i.e., surface-to-volume ratio) can have a significant influence on the amplitude of the Ca^{2+} response, with smaller/thinner dendrites producing greater changes (Holthoff et al., 2002). When we examined TRN dendrites, the diameter did become smaller with increasing distance from soma (Fig. 3*C*) ($r = -0.53$, $p < 0.001$, Pearson's correlation). However, the relationship between the peak Ca^{2+} response and dendritic diameter was weak ($r = -0.21$, $p = 0.05$, Pearson's correlation). This suggests that the smaller dendritic size does not completely account for the larger response observed in distal TRN dendrites. More importantly, this also implies that the density of current across the dendritic tree is not evenly distributed (i.e., higher densities at more distal locations).

Like that of TRN neurons, thalamocortical dendrites also became smaller with increased distance from soma (Fig. 3*D*) (dLGN, $r = -0.66$, $p < 0.001$; VB, $r = -0.73$, $p < 0.001$, Pearson's correlation). However, unlike TRN neurons, VB dendrites

had a threefold stronger inverse relationship between peak Ca^{2+} response and dendritic diameter ($r = -0.67$, $p < 0.001$, Pearson's correlation). This argues that the VB proximal/distal differences (Fig. 2*C*) are primarily attributable to smaller dendritic size and not a larger current density. No significant correlation between peak Ca^{2+} response and dendritic diameter was found for dLGN dendrites ($r = -0.34$, $p = 0.054$, Pearson's correlation). These analyses indicate that the Ca^{2+} distribution in TRN dendrites are fundamentally different from those observed in thalamocortical projection neurons.

For a more quantitative comparison within and across thalamic cell types, we divided dendritic length into five subgroups based on radial distance from soma: soma (0 μm), proximal (15–25 μm), intermediate (50–75 μm), distal I (100–130 μm), and distal II (>150 μm) (Fig. 3*E*). For TRN neurons, the average Ca^{2+} response for each dendritic region was significantly larger than soma ($p < 0.001$, one-way ANOVA with *post hoc* Bonferroni's test) (TRN soma, 5.8 ± 1.6% $\Delta G/R$, $n = 17$N; proximal, 19.5 ± 4.9%, $n = 22$D/17N; intermediate, 25.2 ± 8.9%, $n = 22$D/17N; distal I, 26.7 ± 7.0%, $n = 22$D/17N; distal II, 28.5 ± 7.5%, $n = 14$D/14N). In addition to the somatic/dendritic difference, the Ca^{2+} responses taken from both distal I and distal II locations were significantly larger than proximal ($p < 0.01$, one-way ANOVA with *post hoc* Bonferroni's test). Compared with thalamocortical neurons, TRN neurons had significantly larger Ca^{2+} responses than both dLGN and VB neurons ($p < 0.001$, two-way ANOVA with *post hoc* Bonferroni's test).

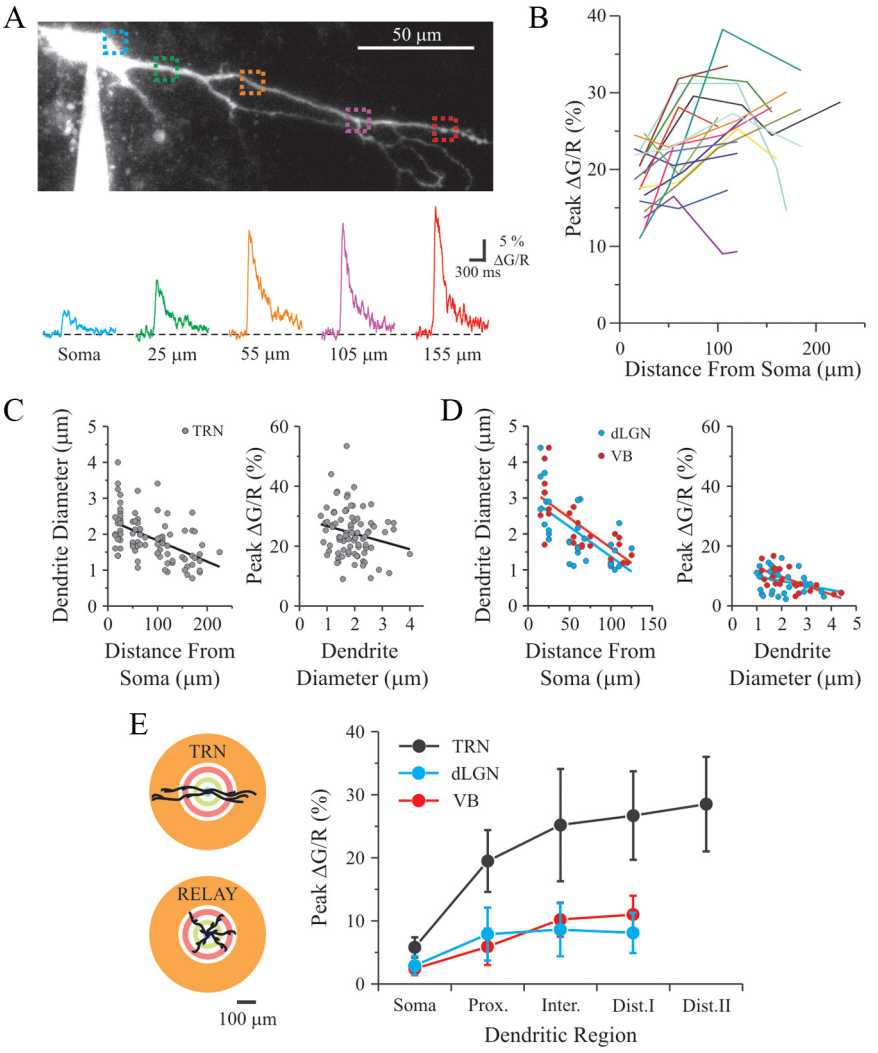

Figure 3. The TRN dendritic/Ca^{2+} relationship is independent of dendritic size. ***A***, Top, Stacked 2PLSM image of an example TRN neuron filled. Boxes indicate where line scans were performed. Bottom, Corresponding Ca^{2+} responses obtained from the neuron above. ***B***, Left, Plot depicts Ca^{2+} responses obtained along 14 different TRN dendrites as a function of dendritic distance. ***C***, Left, Correlation between TRN dendrite diameter and measured distance from soma. Right, Correlation between the peak Ca^{2+} response and the measured TRN dendritic diameter. ***D***, Left, Correlation between dendrite diameter and measured distance from soma for both dLGN (blue) and VB neurons (red). Right, Correlation between Ca^{2+} response and the measured dendritic diameter for both thalamocortical projection neurons. ***E***, Left, Diagram illustrating how data were pooled based on their radial distance from soma (soma, proximal, intermediate, distal I, and distal II). Right, Plot summarizing the average response for the three different thalamic cell types (dLGN: soma, 2.9 ± 2.5%, $n = 7$N; proximal, 7.9 ± 4.2%, $n = 11$D/7N; intermediate, 8.6 ± 4.2%, $n = 13$D/8N; distal I, 8.1 ± 3.2%, $n = 9$D/6N; VB: soma, 2.4 ± 1.0%, $n = 4$N; proximal, 5.9 ± 2.9%, $n = 8$D/4N; intermediate, 10.2 ± 2.7%, $n = 8$D/4N; distal I, 11.0 ± 3.0%, $n = 7$D/4N).

Dendritic Ca^{2+} responses are dependent on firing mode

In many neurons, action potentials initiated in either the axon or soma can backpropagate into the dendritic arbor (Stuart and Sakmann, 1994; Stuart et al., 1997). In pyramidal neurons of the neocortex and hippocampus, backpropagating action potentials have been shown to produce Ca^{2+} responses along their dendrites (Jaffe et al., 1992; Markram et al., 1995; Schiller et al., 1995; Magee and Johnston, 1997). To characterize whether the observed Ca^{2+} responses were possibly evoked by backpropagating action potentials in TRN neurons, we elicited either a single AP or a tonic burst of action potentials (four APs at 100 Hz) using brief somatic current injections (Fig. 4*A*). To ensure TRN neurons were not in burst mode (i.e., deinactivation of I_T), the membrane potential of the soma was adjusted with current to −60 mV. Under these conditions, a single and tonic burst of APs produced a small Ca^{2+} response at proximal dendritic locations (Fig. 4*B*) (single AP, 3.2 ± 2.0% $\Delta G/R$, $n = 6$; tonic burst, 6.1 ± 2.0% $\Delta G/R$, $n = 6$). At more distal locations, the Ca^{2+} responses were difficult to detect from baseline (single AP, 2.3 ± 1.0% $\Delta G/R$, $n = 5$; tonic burst, 2.6 ± 0.9% $\Delta G/R$, $n = 5$). Overall, the dendritic Ca^{2+} responses evoked by action potential discharge at −60 mV were significantly smaller than those produced via a burst discharge at −80 mV (Fig. 4*C*) ($p < 0.001$, two-way ANOVA). These data strongly suggest that an underlying LTS must be responsible for the dendritic Ca^{2+} response.

Dendritic Ca^{2+} responses are mediated by I_T

To determine the nature of the dendritic Ca^{2+} response in TRN neurons, we initially tested whether the burst-induced response was dependent on the activation of voltage-gated Na^+ channels. Using TTX (0.5 μM) to block voltage-gated Na^+ channels, the same somatic current injection revealed a transient, Ca^{2+}-

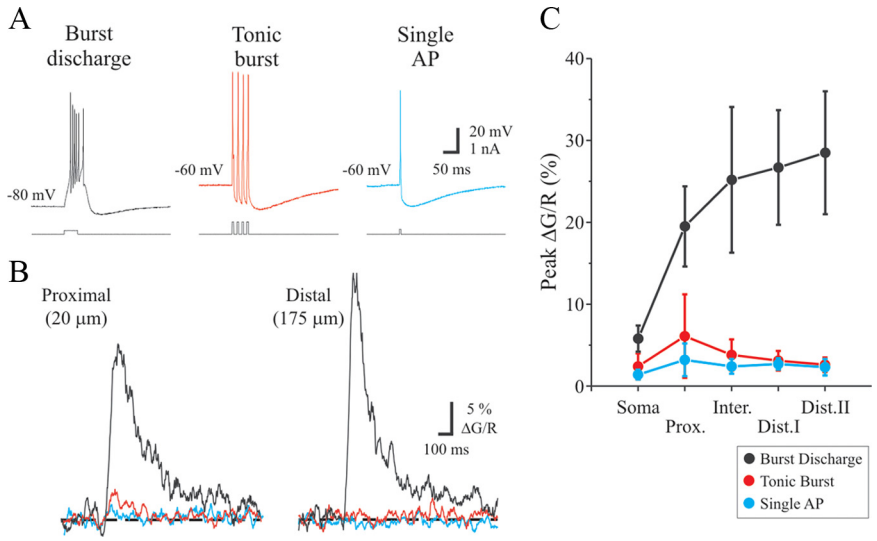

Figure 4. Ca^{2+} responses are dependent on firing mode. ***A***, Action potentials were discharged in one of three ways. Burst discharge (black) was evoked as previously described in Figure 1*B*. A single (blue) or tonic burst (red) of action potentials were evoked by holding the soma near −60 mV and injecting short (5 ms) depolarizing current pulses. A tonic burst consisted of four pulses delivered at 100 Hz. ***B***, Ca^{2+} responses for each of the conditions shown in ***A*** at different distances obtained from the same dendrite. The responses shown are from the same dendrite. ***C***, Plot summarizing the average response to burst discharge (black), tonic burst (red), and single action potential (blue). For reference, the average response to a burst discharge is shown in black.

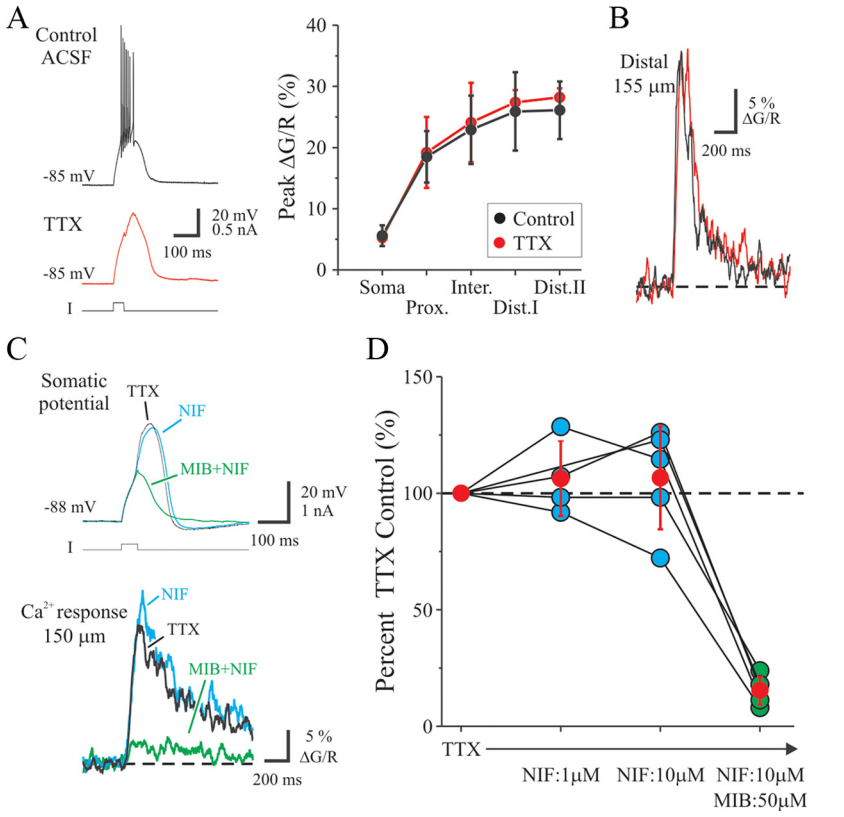

Figure 5. TRN dendritic Ca^{2+} are independent of voltage-gated Na^+ channels but are strongly dependent on voltage-gated T-type Ca^{2+} channels. ***A***, Left, Example of a somatic recording from a TRN neuron in which a depolarizing current step evoked a burst response in control conditions (ACSF) and an LTS after TTX application (red trace). Right, Population graph illustrating the Ca^{2+} responses recorded at different dendritic locations produced by somatic current injection in control conditions (ACSF, black) and in TTX (red). The Ca^{2+} responses in TTX: soma, 5.3 ± 0.7%, n = 4N; proximal, 19.2 ± 5.8%, n = 5D/4N; intermediate, 24.1 ± 6.5%, n = 5D/4N; distal I, 27.4 ± 2.0%, n = 5D/4N; distal II, 28.2 ± 1.5%, n = 5D/5N. ***B***, An example of a Ca^{2+} response obtained from the same location before (black) and after (red) TTX application. ***C***, Top, In TTX, depolarizing current step evokes a LTS (black). Addition of nifedipine (NIF; 10 μM) slightly alters the LTS (blue); however, subsequent addition of MIB (50 μM) strongly attenuates the LTS (green). Bottom, From the same neuron, the control Ca^{2+} response (TTX, black) is slightly changed in the presence of nifedipine (blue) but is almost completely blocked by mibefradil (green). ***D***, Population data for five different distal dendrites (>150 μm) obtained from different TRN neurons. The Ca^{2+} responses are standardized to the response obtained in TTX, and the red data points indicate the mean ± SD.

dependent LTS (Fig. 5*A*). The LTS in turn produced a Ca^{2+} response along the entire length of the dendrite similar to that generated by a burst discharge ($p = 0.84$, two-way ANOVA). To further confirm the independence from voltage-gated Na^+ channels, distal (>150 μm) responses were measured from the same location before and after TTX application. Under these conditions, the magnitude of the response remained the same (Fig. 5*B*: 117.4 ± 34.0% of control, n = 15D/15N, $p = 0.17$, paired t test). These results indicate that, for TRN neurons, the magnitude of the burst-induced dendritic Ca^{2+} response is independent of both the backpropagation of somatic action potentials and dendritic voltage-gated Na^+ channels.

Focusing on the distal dendrites (>150 μm), we next determined which type(s) of voltage-gated Ca^{2+} channels underlie the somatic evoked distal response. While in the presence of TTX (0.5 μM), the addition of the L-type channel blocker nifedipine (1 and 10 μM) reduced the LTS amplitude recorded at the soma (1 μM, ~6% reduction; 10 μM, ~10% reduction) but did not alter the magnitude of the distal Ca^{2+} response (Fig. 5*C*,*D*: 1.0 μM, 106 ± 16% of control, n = 4D/4N, p = 0.5; 10 μM, 107 ± 22.1% of control, n = 5D/5N, $p = 0.7$, paired t test). Subsequent addition of the T-type channel blocker mibefradil (MIB) (40–50 μM) significantly reduced the LTS amplitude recorded at the soma (~39% reduction) and nearly eliminated the distal Ca^{2+} response (MIB, 85.5 ± 6.1% reduction, n = 5D/5N, $p < 0.01$, paired t test). To confirm that the mibefradil block was not affected by nifedipine, we also tested mibefradil alone and observed a similar reduction (MIB alone, 97.5 ± 1.6% reduction, n = 4D/4N, $p < 0.001$, paired t test). Mibefradil also blocked the Ca^{2+} responses at all other dendritic locations (compared with control condition, $p <$ 0.001, two-way ANOVA). Similar to nifedipine, the N,P/Q-type Ca^{2+} channel blocker ω-conotoxin-MVIIC (20–40 nM) did not significantly alter the dendritic Ca^{2+} response (114 ± 21.2% of control, n = 5D/5N, $p = 0.5$, paired t test). Together, these results suggest that the LTS/burst-evoked Ca^{2+} response in TRN dendrites is strongly mediated by the activation of T-type Ca^{2+} channels.

Distal I_T is activated independent of soma/proximal dendrites

Although a distal Ca^{2+} response was always produced with a somatic-evoked LTS/burst, it remained unclear whether

this response was generated by distally located T-type Ca^{2+} channels or was simply the result of the passive invasion of soma/proximal signals into the dendrites. To address this issue directly, individual distal TRN dendrites were stimulated with brief, focal glutamate application (0.5–1.0 mM; 30–50 ms duration) via pressure ejection (Fig. 6*A*). In control conditions [artificial CSF (ACSF)] and holding the soma at a hyperpolarized potential (−80 mV), glutamate application to an individual distal dendrite (>125 μm) generated a strong burst discharge recorded at the soma (Fig. 6*B*). After the addition of TTX (0.5 μM), the same application of glutamate now produced an LTS (Fig. 6*B*, TTX). No discernable difference was detected between the glutamate-evoked burst/LTS and those generated via somatic current injection (APs per burst: soma current injection, 3.1 ± 2.1 APs; glutamate, 3.2 ± 2.0 APs, $n = 9$, $p = 0.25$, paired t test; LTS amplitude: soma current injection, 43.1 ± 5.8 mV; glutamate, 43.9 ± 4.9 mV, $n = 9$, $p = 0.30$, paired t test). When the soma was depolarized to inactivate soma/proximal I_T (−60 mV), distal glutamate application resulted in a much smaller, EPSP-like depolarization (Fig. 6*B*: −80 mV, 44.9 ± 4.2 mV; −60 mV, 11.0 ± 4.4 mV; $n = 8$, $p < 0.001$, paired t test). These data suggest that distal afferent signals are capable, when the appropriate voltage-dependent conditions are present at the soma, of generating a burst/LTS output from the neuron.

When examining the glutamate-evoked Ca^{2+} response, there was a clear relationship between the response magnitude and the success/failure of generating a somatic LTS (Fig. 6*C*). When a subthreshold application of glutamate was ejected, it produced a small depolarization at the soma with little or no distal Ca^{2+} response (Fig. 6*C*, red traces); however, a large dendritic response was always associated with a suprathreshold application of glutamate, which in turn always produced an LTS at the soma (Fig. 6*C*, black traces). More importantly, regardless of whether the somatic membrane potential was held at a hyperpolarized (−80 mV) or depolarized (−60 mV) level, suprathreshold glutamate application always produced a robust Ca^{2+} response in the distal dendrites (Fig. 6*D*). Compared with the Ca^{2+} response elicited by a somatic current injection, the glutamate-evoked response was prolonged. The amplitude of the glutamate-evoked response at −80 mV (24.0 ± 7.0% $\Delta G/R$) was larger than both the somatic-evoked (19.8 ± 9.1% $\Delta G/R$, $p < 0.05$, paired t test) and the glutamate-evoked (18.3 ± 6.3% $\Delta G/R$, $n = 12$, $p < 0.001$, paired t test) response at −60 mV (Fig. 6*E*). No significant difference was found between the somatic-evoked and glutamate-evoked response at −60 mV ($p = 0.34$, paired t test). These results indicate that focal glutamate application to a distal dendrite is sufficient to activate a large distal Ca^{2+} response independent of soma/proximal dendrites.

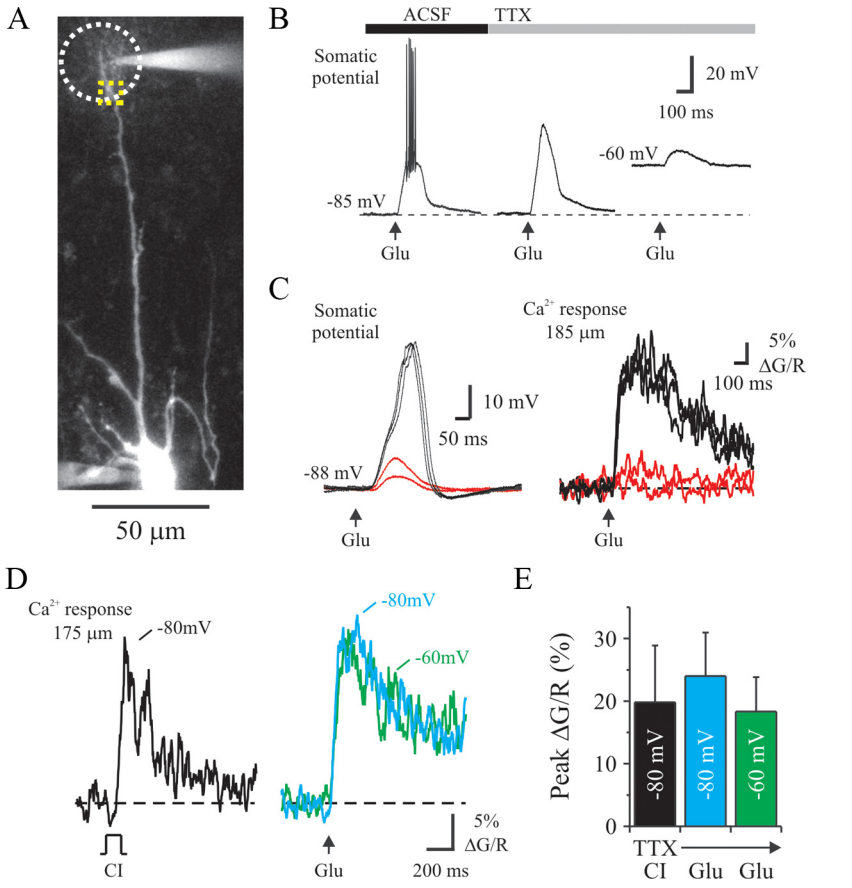

Figure 6. Focal glutamate application onto a distal dendrite evokes local Ca^{2+} current independent of the soma/proximal dendrites. ***A***, Stacked 2PLSM image of a TRN neuron filled and pressure-ejection pipette near a distal dendrite (185 μm). The pipette contained glutamate (0.5–1 mM in ACSF) and Alexa Fluor 594 (12.5 μM), the latter aiding in the placement of the pipette and estimating the spread of glutamate ejection, which is represented by the white-dotted line (~15–20 μm radius). Line scans were performed near the edge of the stimulated area (yellow box). ***B***, Glutamate application (Glu) to distal dendrite produced a burst discharge recorded at the soma in control conditions (ACSF). In TTX (0.5 μM), glutamate produced an LTS when the cell was initially held at −85 mV, but when the cell was depolarized (−60 mV), the same stimulation produced a small transient depolarization (EPSP-like). ***C***, Left, Somatic response to five separate glutamate applications with different puff intensities (0.75–3 psi, 50 ms duration). Right, Corresponding Ca^{2+} responses recorded near the glutamate pipette. Two subthreshold (red) and three suprathreshold (black) responses are shown. ***D***, Examples of Ca^{2+} responses measured at a distal dendrite (175 μm) in the presence of TTX resulting from somatic current injection (CI; black trace) and distal glutamate application. The latter Ca^{2+} responses depict glutamate-evoked responses when the soma was held at either −80 mV (blue) or −60 mV (red). ***E***, The plot illustrates the amplitude of the glutamate-evoked responses in these two conditions (−85 or −60 mV at soma) relative to the Ca^{2+} responses evoked by somatic current injection.

Considering that glutamate stimulation could activate Ca^{2+}-permeable NMDA receptors, we tested the antagonist CPP on the glutamate-evoked distal Ca^{2+} response. Bath application of CPP (10–20 μM) produced a small but statistically significant attenuation of the glutamate-evoked Ca^{2+} response (Fig. 7*A*) (glutamate–control, 36.9 ± 6.6% $\Delta G/R$; glutamate–TTX + CPP, 31.6 ± 5.8% $\Delta G/R$; $n = 8$, $p < 0.05$, paired t test). Importantly, the glutamate-evoked Ca^{2+} response in the presence of CPP did not differ from the response evoked by somatic current injection (30.2 ± 8.2% $\Delta G/R$; $n = 8$, $p = 0.50$, paired t test). In all eight neurons tested, CPP also reduced the prolonged Ca^{2+} response observed with glutamate application. The subsequent application of the AMPA receptor antagonist DNQX (20–40 μM) eliminated the glutamate-evoked Ca^{2+} response (CPP + DNQX, 5.0 ± 5.8% $\Delta G/R$; $n = 3$). Neither CPP nor CPP + DNQX altered the dendritic Ca^{2+} responses evoked by somatic current injection ($p = 0.92$, $n = 7$, paired t test and $p = 0.93$, $n = 6$, paired t test, respectively).

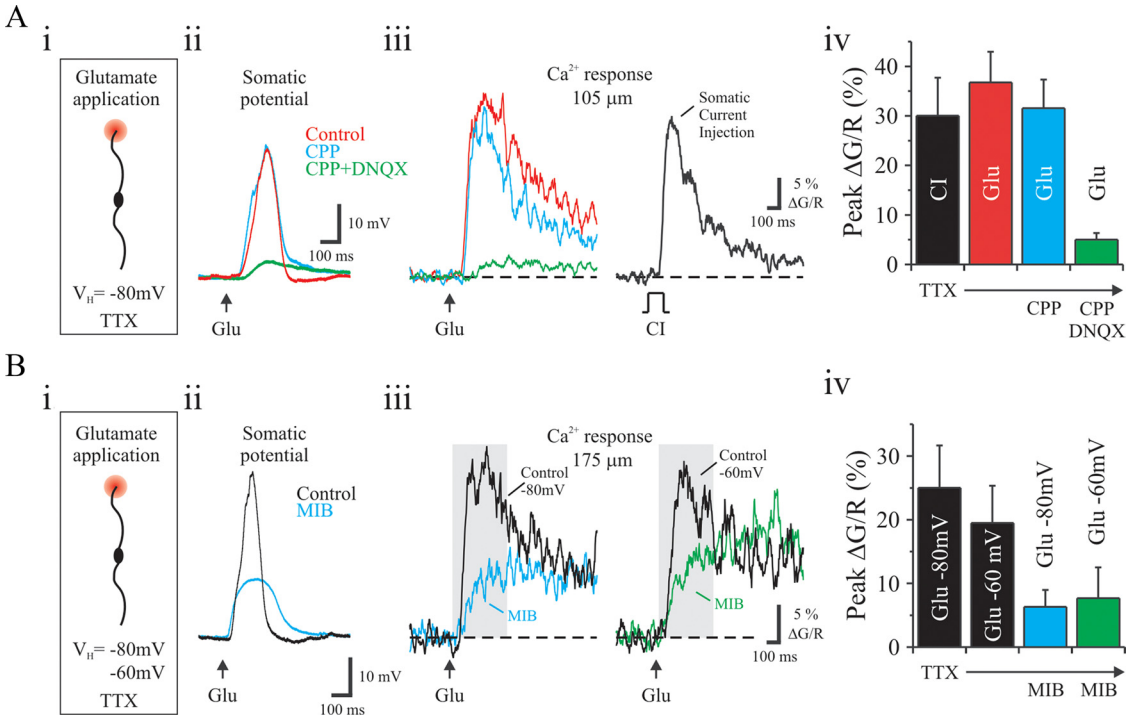

Figure 7. Characterization of glutamate-evoked distal Ca^{2+} signals. ***Ai***, Experimental design consisted of applying glutamate (Glu) to an individual distal TRN dendrite while holding the soma at −80 mV in a bath solution that contained TTX (0.5 µM). ***Aii***, Glutamate-evoked response recorded at the soma before (Control) and after CPP or CPP + DNQX application. ***Aiii***, Left, In the same cell as ***Aii***, the corresponding glutamate-evoked Ca^{2+} response imaged at a distal location. Right, For reference, an LTS Ca^{2+} response evoked by a somatic current injection (CI) is shown. ***Aiv***, Average amplitude of the Ca^{2+} response for each of the four conditions tested are plotted. ***Bi***, Experimental design consisted of applying glutamate (Glu) to an individual distal TRN dendrite while holding the soma at either −80 or −60 mV in a bath solution that contained TTX (0.5 µM). ***Bii***, Glutamate-evoked response recorded at the soma while holding at −80 mV before (Control) and after mibefradil (MIB; 50 µM) application. ***Biii***, Control trace (black) is the response to distal glutamate application in presence of TTX (left, −80 mV; right, −60 mV). After the addition of mibefradil, the subsequent Ca^{2+} responses to glutamate application are significantly reduced. Peak Ca^{2+} responses for this experiment were measured within the gray box. ***Biv***, Average amplitude of the Ca^{2+} response for each of the four conditions tested are plotted.

We next tested the contribution of T-type Ca^{2+} channels on the glutamate-evoked Ca^{2+} response (Fig. 7*B*). In mibefradil (50 µM), the amplitude of the glutamate-evoked dendritic Ca^{2+} responses were significantly reduced regardless of the somatic membrane potential (at −80 mV: control, 25.0 ± 6.6% Δ*G*/*R*, $n = 5$; with MIB, 6.3 ± 2.6% Δ*G*/*R*, $n = 5$, $p < 0.01$, paired *t* test; at −60 mV: control, 19.5 ± 5.9% Δ*G*/*R*, $n = 4$; with MIB, 7.7 ± 4.8% Δ*G*/*R*, $n = 4$, $p < 0.01$, paired *t* test). These findings suggest that distal glutamate application to an individual TRN dendrite is sufficient to activate local T-type Ca^{2+} channels. Considering that mibefradil reduced both the distal Ca^{2+} response and corresponding somatic depolarization (58 and 12% reduction at −80 and −60 mV, respectively), it is likely that I_T is amplifying afferent input.

Synaptic activation of distal I_T

To probe the functional relevance of distal I_T amplification, we stimulated local excitatory synaptic afferents in place of glutamate application. For these experiments, the stimulating electrode was positioned lateral to the TRN within the internal capsule so to activate both corticothalamic and thalamocortical fibers (Golshani et al., 2001; Zhang and Jones, 2004). Using a single stimulus (40–300 µA, 500 µs, 0.1 Hz), burst discharge was generated in our somatic recording when the neuron was held at −80 mV, along with a corresponding large distal Ca^{2+} response (Fig. 8*A*). The magnitude of the synaptically evoked distal Ca^{2+} response did not differ from the response evoked by somatic current injection (at −80 mV: synaptic, 27.6 ± 4.0% Δ*G*/*R*; soma current injection, 23.7 ± 6.9% Δ*G*/*R*, $n = 4$, $p = 0.23$, paired *t* test). Subsequent application of CPP (20 µM) did not significantly alter the amplitude of the synaptically evoked Ca^{2+} response (with CPP, 23.1 ± 10.7% Δ*G*/*R*, $n = 4$, $p = 0.28$, paired *t* test); however, addition of DNQX (40 µM) eliminated the response (CPP + DNQX, 2.0 ± 0.4% Δ*G*/*R*, $n = 4$, $p < 0.001$, paired *t* test). When the soma was depolarized to −60 mV, the same stimulus generated one to two action potentials (Fig. 8*B*). Under these conditions, the amplitude of the synaptically evoked Ca^{2+} response displayed a considerable degree of variability (45.9% coefficient of variation, $n = 4$); however, the large responses generated (21.1 ± 8.3% Δ*G*/*R*, $n = 4$) were not statistically different from the responses generated by a somatic induced LTS (23.7 ± 6.9% Δ*G*/*R*, $p = 0.48$, paired *t* test). Subsequent bath application of CPP (20 µM) did not alter the amplitude of the Ca^{2+} response (with CPP, 17.2 ± 12.7% Δ*G*/*R*, $n = 4$, $p = 0.36$, paired *t* test), whereas DNQX eliminated the response (1.5 ± 0.5% Δ*G*/*R*, $n = 4$, $p < 0.02$, paired *t* test).

Discussion

The results of the present study indicate that a somatic burst discharge or activation of an LTS can evoke a robust Ca^{2+} response in TRN dendrites mediated by I_T. Ca^{2+} influx was observed along the entire length of the dendrite, with the largest response typically occurring at more distal locations (>100 µm). Although all thalamic neurons tested produced a change in dendritic Ca^{2+} in response to burst discharge, the magnitude within TRN dendrites was significantly larger than those observed in thalamocortical relay neurons. In addition, we show that distally located I_T can be activated independently from the soma/proximal dendrites, therefore possibly serving to boost local afferent

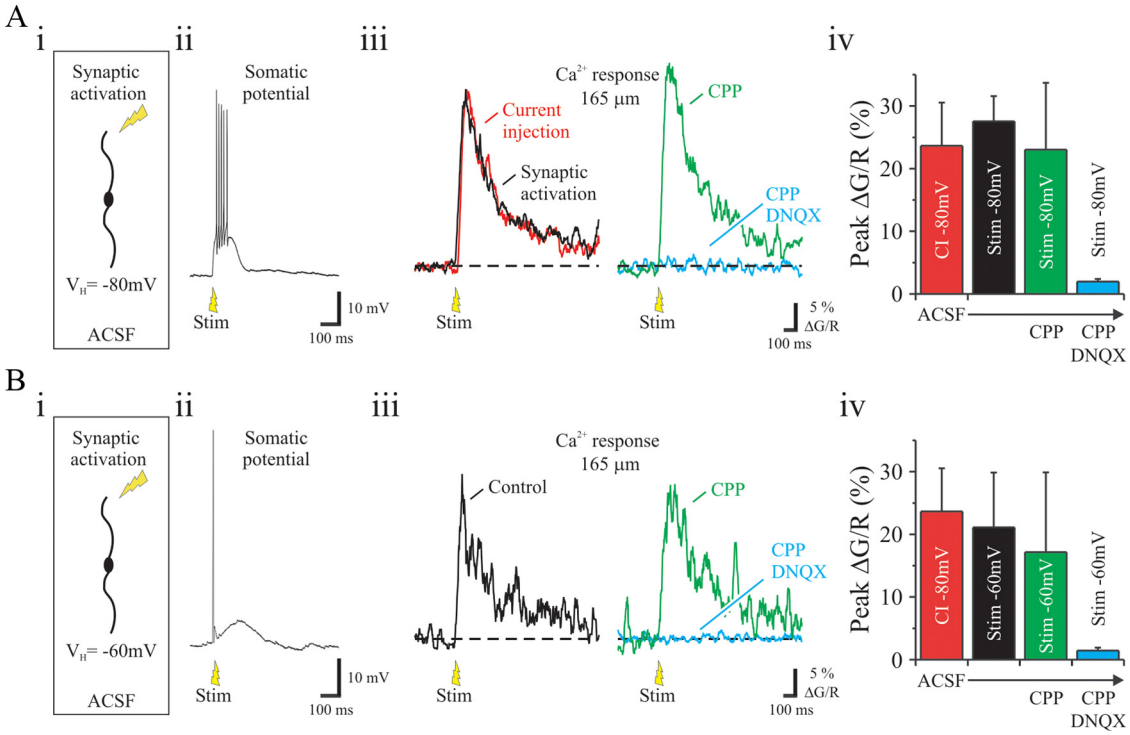

Figure 8. Characterization of synaptic-evoked distal Ca^{2+} signals. ***Ai***, Experimental design consisted of stimulating the internal capsule using a single stimulus (Stim) while holding TRN neurons the soma at −80 in a control ACSF bath solution. ***Aii***, Somatic recording of a synaptically evoked burst discharge while holding at −80 mV. ***Aiii***, Left, Distal Ca^{2+} response evoked by synaptic stimulation of the internal capsule (black). For reference, a control (red) response to a somatic current injection (CI) is also shown. Right, Resulting synaptically evoked Ca^{2+} responses after the bath application of CPP (green) and CPP + DNQX (blue). ***Aiv***, Average amplitude of the Ca^{2+} response for each of the four conditions tested are plotted. ***Bi***, Experimental design consisted of stimulating the internal capsule using a single stimulus (Stim) while holding TRN neurons the soma at −60 mV in a control ACSF bath solution. ***Bii***, Somatic recording of a synaptically evoked burst discharge while holding at −60 mV. ***Biii***, Left, A single Ca^{2+} response (black) evoked by synaptic stimulation of the internal capsule. Subsequent Ca^{2+} responses after bath application of CPP (green) and CPP + DNQX (blue). ***Biv***, Average amplitude of the Ca^{2+} response for each of the four conditions tested are plotted.

inputs onto TRN neurons. The activation of distal I_T, by either focal glutamate application or synaptic activation, required activation of AMPA but not NMDA glutamate receptors. Considering that I_T kinetics and amplitude are temperature dependent (Coulter et al., 1989; Takahashi et al., 1991), performing these experiments at room temperature have likely altered the typical physiological response observed at body temperature but may have also provided a more accurate measurement of the peak change (Markram et al., 1995). Overall, these findings provide the first physiological evidence of the somatodendritic distribution of I_T in TRN neurons, as well as insight regarding the potential functional role of I_T in synaptic integration within reticular neurons.

Somatodendritic distribution of I_T in TRN neurons

It is well documented that activation of I_T and the resulting LTS are responsible for generating a burst discharge of action potentials in TRN and thalamocortical relay neurons (Llinás and Jahnsen, 1982; Deschênes et al., 1984; Jahnsen and Llinás, 1984; Domich et al., 1986; Avanzini et al., 1989; Coulter et al., 1989; Crunelli et al., 1989; Hernández-Cruz and Pape, 1989; Suzuki and Rogawski, 1989; Huguenard and Prince, 1992). However, data regarding the dendritic distribution of I_T in the thalamus have been limited to studies focusing on thalamocortical relay neurons (Munsch et al., 1997; Zhou et al., 1997; Destexhe et al., 1998; Williams and Stuart, 2000). For the TRN neuron, any accurate physiological quantification of the distribution of I_T has been lacking. The results of the present study indicate a heterogeneous dendritic distribution of I_T in TRN neurons, results that are consistent with a previous computational study (Destexhe et al., 1996). Although an accurate quantification of T-type channel density is difficult to extrapolate, the weak correlation between Ca^{2+} response amplitude and dendritic diameter implies an increased density at more distal locations (Fig. 3*C*). This interpretation corresponds well with a recent anatomical study that found a higher density of T-type Ca^{2+} channels in small-diameter TRN dendrites, likely representing distal dendrites (Kovács et al., 2010).

State-dependent amplification

Our findings also support the general hypothesis that I_T may serve to amplify afferent input as suggested in different neuronal types (Magee et al., 1995; Gillessen and Alzheimer, 1997; Williams et al., 1997; Urban et al., 1998; Watanabe et al., 1998; Williams and Stuart, 2000; Goldberg et al., 2004). Considering the voltage dependence of I_T, namely being activated from relatively hyperpolarized potentials, a non-uniform membrane potential along the somatodendritic axis could have significant influence on dendritic excitability, synaptic amplification, and ultimately action potential output. For example, if the somatodendritic axis is uniformly hyperpolarized, amplified distal input would be uninterrupted and actively propagated toward the soma, ultimately producing a burst discharge. Conversely, if the soma/proximal dendrites were depolarized relative to the distal dendrites, distal signals would still be amplified considering activation of I_T, resulting in a larger afferent EPSP at the soma level but not producing a burst discharge. In the later scenario, synapses located further from the soma would still have an ability to contribute to

somatic output given sufficient activation of distal I_T. Finally, different neuromodulators thought to depolarize TRN via actions at distal dendrites (e.g., cholecystokinin, glutamate via metabotropic receptors) could inactivate I_T and thereby dampen afferent inputs by attenuating the amplification by I_T (Cox et al., 1995; Sohal et al., 1998). Thus, at the dendritic level, I_T could serve to regulate the spatial integrative properties of the TRN neuron and interactions between distinct dendritic compartments (i.e., proximal/soma and distal).

Given that TRN neurons can have multiple primary dendritic branches (Scheibel and Scheibel, 1966; Jones, 1975; Lübke, 1993; Ohara and Havton, 1996), an interesting and potentially important issue is whether or not the voltage state across the somatodendritic axis could differ between individual dendrites of the same TRN neuron. Such dendritic isolation could promote highly localized processing and would allow individual branches to act as independent integrators of different information (Euler et al., 2002; Häusser and Mel, 2003).

Heterogeneity among TRN neurons

Although this study focused on the functional role of dendritic I_T in TRN neurons capable of burst discharge, there are studies that have clearly identified a subpopulation of nonbursting TRN neurons (Contreras et al., 1992; Brunton and Charpak, 1997; Lee et al., 2007). For these neurons, the lack of burst discharge seems to result from a minimal amount of I_T recorded at the soma. However, the inability to induce a somatic burst discharge does not suggest a complete absences of dendritic I_T. It is possible that nonbursting TRN neurons could represent a subpopulation with an extreme proximal–distal difference in their distribution of I_T. In theory, maintaining a high density of distal I_T would still allow for the amplification of distal afferent input with the lack of soma/proximal I_T preventing the neuron from generating a burst response. In fact, a more distal distribution of I_T in nonbursting TRN neurons is supported by the fact that in a subset of these neurons a small LTS could be unmasked when a K^+-channel blocker was applied (Lee et al., 2007). Although such a somatodendritic distribution remains to be tested, the functional consequence of such a distribution may play an important role in the transfer of modality-specific information as well as thalamocortical operations.

Functional significance of distal I_T

Considering the functional architecture of the TRN, elongated nature of TRN dendrites, and robust responses in distal processes, could distal dendrites serve as sites of intense integration within and across different modalities? The TRN is situated at the interface between the thalamus and neocortex and receives collateral innervation from both thalamocortical and corticothalamic projection neurons. As the fibers pass through the TRN, they assemble in several well defined modality-related sectors (Jones, 1975; Montero, 1997; Guillery and Harting, 2003). Furthermore, sectors can be subdivided into slabs that receive afferent information from focal areas of the neocortex and dorsal thalamus or slabs of TRN neurons projecting to specific regions of the dorsal thalamus (Crabtree, 1999).

Because most TRN neurons possess elongated dendrites (Scheibel and Scheibel, 1966; Jones, 1975; Lübke, 1993; Ohara and Havton, 1996), it is likely that neurons near the borders would have some distal dendrites cross into neighboring sectors or slabs. Because the majority of afferent inputs onto distal dendrites arise from corticothalamic neurons (Liu et al., 1995), it is possible that a strong "top-down" modulation of distal TRN dendrites would significantly influence the integrative properties of the TRN by altering the resting voltage-state of the somatodendritic axis. Such top-down modulation could arise from one or a combination of inputs originating from either the primary sensory neocortex (Montero, 2000) or prefrontal cortex (Zikopoulos and Barbas, 2006). Ultimately, the degree of top-down influence onto distal dendrites could dictate the degree in which the TRN gates "bottom-up" information transfer within and/or across different modalities.

Another potential function of distal dendritic I_T is that such mechanisms could serve to facilitate intra-TRN communication. Considering that many TRN neurons are coupled by electrical synapses (Landisman et al., 2002; Long et al., 2004; Landisman and Connors, 2005) and the electrical signals through these synapses are subjected to severe attenuation and low-pass filtering (Galarreta and Hestrin, 2001), it is possible that high densities of distal I_T could also serve to amplify dendritic electrical synapses among TRN neurons and thereby facilitate intra-TRN communication in a state-dependent manner. It is also intriguing to speculate as to whether I_T and electrical synapses could help generate and preserve the endogenous spindle rhythmic activity observed in the isolated TRN *in vivo* (Steriade et al., 1987). Furthermore, given the possibility of dendrodendritic synapses within cat TRN neurons, distal I_T could strongly influence such communication if present in rodents (Deschênes et al., 1985). The fact that we did not observe strong distal Ca^{2+} responses in relay neurons and they are not electrically coupled in the relatively mature animal (Lee et al., 2010) further supports this possibility.

To date, there are limited reports of *in vivo* electrophysiological recordings of TRN neurons responding to more than one sensory modality (Sugitani, 1979; Shosaku and Sumitomo, 1983). However, recent studies indicate that TRN activity is subjected to cross-modal modulation (Yu et al., 2009) and may be affected by various attentional demands (McAlonan et al., 2006, 2008; Yu et al., 2009). In conjunction with our results, we speculate that the contribution of distal dendrites may underlie such cross-modal actions in a state-dependent manner. Clearly, the resting state of the dendrites and distribution of I_T will have significant influence on thalamocortical operations that requires future investigation.

References

Avanzini G, de Curtis M, Panzica F, Spreafico R (1989) Intrinsic properties of nucleus reticularis thalami neurones of the rat studied in vitro. J Physiol 416:111–122.

Brunton J, Charpak S (1997) Heterogeneity of cell firing properties and opioid sensitivity in the thalamic reticular nucleus. Neuroscience 78:303–307.

Contreras D, Curró Dossi R, Steriade M (1992) Bursting and tonic discharges in two classes of reticular thalamic neurons. J Neurophysiol 68:973–977.

Contreras D, Curró Dossi R, Steriade M (1993) Electrophysiological properties of cat reticular thalamic neurones in vivo. J Physiol 470:273–294.

Coulter DA, Huguenard JR, Prince DA (1989) Calcium currents in rat thalamocortical relay neurones: kinetic properties of the transient, low-threshold current. J Physiol 414:587–604.

Cox CL, Huguenard JR, Prince DA (1995) Cholecystokinin depolarizes rat thalamic reticular neurons by suppressing a K^+ conductance. J Neurophysiol 74:990–1000.

Cox CL, Huguenard JR, Prince DA (1997) Nucleus reticularis neurons mediate diverse inhibitory effects in thalamus. Proc Natl Acad Sci U S A 94:8854–8859.

Crabtree JW (1999) Intrathalamic sensory connections mediated by the thalamic reticular nucleus. Cell Mol Life Sci 56:683–700.

Crabtree JW, Isaac JT (2002) New intrathalamic pathways allowing

modality-related and cross-modality switching in the dorsal thalamus. J Neurosci 22:8754–8761.

Crabtree JW, Collingridge GL, Isaac JT (1998) A new intrathalamic pathway linking modality-related nuclei in the dorsal thalamus. Nat Neurosci 1:389–394.

Crick F (1984) Function of the thalamic reticular complex: the searchlight hypothesis. Proc Natl Acad Sci U S A 81:4586–4590.

Crunelli V, Lightowler S, Pollard CE (1989) A T-type Ca^{2+} current underlies low-threshold Ca^{2+} potentials in cells of the cat and rat lateral geniculate nucleus. J Physiol 413:543–561.

Cueni L, Canepari M, Luján R, Emmenegger Y, Watanabe M, Bond CT, Franken P, Adelman JP, Lüthi A (2008) T-type Ca^{2+} channels, SK2 channels and SERCAs gate sleep-related oscillations in thalamic dendrites. Nat Neurosci 11:683–692.

Deschênes M, Paradis M, Roy JP, Steriade M (1984) Electrophysiology of neurons of lateral thalamic nuclei in cat: resting properties and burst discharges. J Neurophysiol 51:1196–1219.

Deschênes M, Madariaga-Domich A, Steriade M (1985) Dendrodendritic synapses in the cat reticularis thalami nucleus: a structural basis for thalamic spindle synchronization. Brain Res 334:165–168.

Destexhe A, Contreras D, Steriade M, Sejnowski TJ, Huguenard JR (1996) In vivo, in vitro, and computational analysis of dendritic calcium currents in thalamic reticular neurons. J Neurosci 16:169–185.

Destexhe A, Neubig M, Ulrich D, Huguenard J (1998) Dendritic low-threshold calcium currents in thalamic relay cells. J Neurosci 18:3574–3588.

Domich L, Oakson G, Steriade M (1986) Thalamic burst patterns in the naturally sleeping cat: a comparison between cortically projecting and reticularis neurones. J Physiol 379:429–449.

Euler T, Detwiler PB, Denk W (2002) Directionally selective calcium signals in dendrites of starburst amacrine cells. Nature 418:845–852.

Galarreta M, Hestrin S (2001) Electrical synapses between GABA-releasing interneurons. Nat Rev Neurosci 2:425–433.

Gillessen T, Alzheimer C (1997) Amplification of EPSPs by low Ni^{2+}- and amiloride-sensitive Ca^{2+} channels in apical dendrites of rat CA1 pyramidal neurons. J Neurophysiol 77:1639–1643.

Goldberg JH, Lacefield CO, Yuste R (2004) Global dendritic calcium spikes in mouse layer 5 low threshold spiking interneurones: implications for control of pyramidal cell bursting. J Physiol 558:465–478.

Golshani P, Liu XB, Jones EG (2001) Differences in quantal amplitude reflect GluR4-subunit number at corticothalamic synapses on two populations of thalamic neurons. Proc Natl Acad Sci U S A 98:4172–4177.

Govindaiah, Cox CL (2004) Synaptic activation of metabotropic glutamate receptors regulates dendritic outputs of thalamic interneurons. Neuron 41:611–623.

Guillery RW, Harting JK (2003) Structure and connections of the thalamic reticular nucleus: advancing views over half a century. J Comp Neurol 463:360–371.

Häusser M, Mel B (2003) Dendrites: bug or feature? Curr Opin Neurobiol 13:372–383.

Hernández-Cruz A, Pape HC (1989) Identification of two calcium currents in acutely dissociated neurons from the rat lateral geniculate nucleus. J Neurophysiol 61:1270–1283.

Holthoff K, Tsay D, Yuste R (2002) Calcium dynamics of spines depend on their dendritic location. Neuron 33:425–437.

Huguenard JR (1996) Low-threshold calcium currents in central nervous system neurons. Annu Rev Physiol 58:329–348.

Huguenard JR, Prince DA (1992) A novel T-type current underlies prolonged Ca^{2+}-dependent burst firing in GABAergic neurons of rat thalamic reticular nucleus. J Neurosci 12:3804–3817.

Jaffe DB, Johnston D, Lasser-Ross N, Lisman JE, Miyakawa H, Ross WN (1992) The spread of Na^{+} spikes determines the pattern of dendritic Ca^{2+} entry into hippocampal neurons. Nature 357:244–246.

Jahnsen H, Llinás R (1984) Ionic basis for the electro-responsiveness and oscillatory properties of guinea-pig thalamic neurones in vitro. J Physiol 349:227–247.

Joksovic PM, Bayliss DA, Todorovic SM (2005) Different kinetic properties of two T-type Ca^{2+} currents of rat reticular thalamic neurones and their modulation by enflurane. J Physiol 566:125–142.

Jones EG (1975) Some aspects of the organization of the thalamic reticular complex. J Comp Neurol 162:285–308.

Kim U, Sanchez-Vives MV, McCormick DA (1997) Functional dynamics of GABAergic inhibition in the thalamus. Science 278:130–134.

Kovács K, Sík A, Ricketts C, Timofeev I (2010) Subcellular distribution of low-voltage activated T-type Ca^{2+} channel subunits ($Ca_v3.1$ and $Ca_v3.3$) in reticular thalamic neurons of the cat. J Neurosci Res 88:448–460.

Landisman CE, Connors BW (2005) Long-term modulation of electrical synapses in the mammalian thalamus. Science 310:1809–1813.

Landisman CE, Long MA, Beierlein M, Deans MR, Paul DL, Connors BW (2002) Electrical synapses in the thalamic reticular nucleus. J Neurosci 22:1002–1009.

Lee SC, Cruikshank SJ, Connors BW (2010) Electrical and chemical synapses between relay neurons in developing thalamus. J Physiol 588:2403–2415.

Lee SH, Govindaiah G, Cox CL (2007) Heterogeneity of firing properties among rat thalamic reticular nucleus neurons. J Physiol 582:195–208.

Lee SM, Friedberg MH, Ebner FF (1994a) The role of GABA-mediated inhibition in the rat ventral posterior medial thalamus. I. Assessment of receptive field changes following thalamic reticular nucleus lesions. J Neurophysiol 71:1702–1715.

Lee SM, Friedberg MH, Ebner FF (1994b) The role of GABA-mediated inhibition in the rat ventral posterior medial thalamus. II. Differential effects of GABAA and GABAB receptor antagonists on responses of VPM neurons. J Neurophysiol 71:1716–1726.

Liu XB, Jones EG (1999) Predominance of corticothalamic synaptic inputs to thalamic reticular nucleus neurons in the rat. J Comp Neurol 414:67–79.

Liu XB, Warren RA, Jones EG (1995) Synaptic distribution of afferents from reticular nucleus in ventroposterior nucleus of cat thalamus. J Comp Neurol 352:187–202.

Llinás R, Jahnsen H (1982) Electrophysiology of mammalian thalamic neurones in vitro. Nature 297:406–408.

Long MA, Landisman CE, Connors BW (2004) Small clusters of electrically coupled neurons generate synchronous rhythms in the thalamic reticular nucleus. J Neurosci 24:341–349.

Lübke J (1993) Morphology of neurons in the thalamic reticular nucleus (TRN) of mammals as revealed by intracellular injections into fixed brain slices. J Comp Neurol 329:458–471.

Magee JC, Johnston D (1997) A synaptically controlled, associative signal for Hebbian plasticity in hippocampal neurons. Science 275:209–213.

Magee JC, Christofi G, Miyakawa H, Christie B, Lasser-Ross N, Johnston D (1995) Subthreshold synaptic activation of voltage-gated Ca^{2+} channels mediates a localized Ca^{2+} influx into the dendrites of hippocampal pyramidal neurons. J Neurophysiol 74:1335–1342.

Markram H, Helm PJ, Sakmann B (1995) Dendritic calcium transients evoked by single back-propagating action potentials in rat neocortical pyramidal neurons. J Physiol 485:1–20.

McAlonan K, Cavanaugh J, Wurtz RH (2006) Attentional modulation of thalamic reticular neurons. J Neurosci 26:4444–4450.

McAlonan K, Cavanaugh J, Wurtz RH (2008) Guarding the gateway to cortex with attention in visual thalamus. Nature 456:391–394.

Montero VM (1997) c-fos induction in sensory pathways of rats exploring a novel complex environment: shifts of active thalamic reticular sectors by predominant sensory cues. Neuroscience 76:1069–1081.

Montero VM (2000) Attentional activation of the visual thalamic reticular nucleus depends on "top-down" inputs from the primary visual cortex via corticogeniculate pathways. Brain Res 864:95–104.

Munsch T, Budde T, Pape HC (1997) Voltage-activated intracellular calcium transients in thalamic relay cells and interneurons. Neuroreport 8:2411–2418.

Ohara PT, Havton LA (1996) Dendritic arbors of neurons from different regions of the rat thalamic reticular nucleus share a similar orientation. Brain Res 731:236–240.

Ohara PT, Lieberman AR (1981) Thalamic reticular nucleus: anatomical evidence that cortico-reticular axons establish monosynaptic contact with reticulo-geniculate projection cells. Brain Res 207:153–156.

Sabatini BL, Oertner TG, Svoboda K (2002) The life cycle of Ca^{2+} ions in dendritic spines. Neuron 33:439–452.

Scheibel ME, Scheibel AB (1966) The organization of the nucleus reticularis thalami: a Golgi study. Brain Res 1:43–62.

Schiller J, Helmchen F, Sakmann B (1995) Spatial profile of dendritic calcium transients evoked by action potentials in rat neocortical pyramidal neurones. J Physiol 487:583–600.

Shosaku A, Sumitomo I (1983) Auditory neurons in the rat thalamic reticular nucleus. Exp Brain Res 49:432–442.

Sohal VS, Cox CL, Huguenard JR (1998) Localization of CCK receptors in thalamic reticular neurons: a modeling study. J Neurophysiol 79:2820–2824.

Spreafico R, de Curtis M, Frassoni C, Avanzini G (1988) Electrophysiological characteristics of morphologically identified reticular thalamic neurons from rat slices. Neuroscience 27:629–638.

Steriade M, Domich L, Oakson G (1986) Reticularis thalami neurons revisited: activity changes during shifts in states of vigilance. J Neurosci 6:68–81.

Steriade M, Domich L, Oakson G, Deschênes M (1987) The deafferented reticular thalamic nucleus generates spindle rhythmicity. J Neurophysiol 57:260–273.

Steriade M, McCormick DA, Sejnowski TJ (1993) Thalamocortical oscillations in the sleeping and aroused brain. Science 262:679–685.

Stuart G, Spruston N, Sakmann B, Häusser M (1997) Action potential initiation and backpropagation in neurons of the mammalian CNS. Trends Neurosci 20:125–131.

Stuart GJ, Sakmann B (1994) Active propagation of somatic action potentials into neocortical pyramidal cell dendrites. Nature 367:69–72.

Sugitani M (1979) Electrophysiological and sensory properties of the thalamic reticular neurones related to somatic sensation in rats. J Physiol 290:79–95.

Suzuki S, Rogawski MA (1989) T-type calcium channels mediate the transition between tonic and phasic firing in thalamic neurons. Proc Natl Acad Sci U S A 86:7228–7232.

Takahashi K, Ueno S, Akaike N (1991) Kinetic properties of T-type Ca^{2+} currents in isolated rat hippocampal CA1 pyramidal neurons. J Neurophysiol 65:148–155.

Urban NN, Henze DA, Barrionuevo G (1998) Amplification of perforant-path EPSPs in CA3 pyramidal cells by LVA calcium and sodium channels. J Neurophysiol 80:1558–1561.

Watanabe S, Takagi H, Miyasho T, Inoue M, Kirino Y, Kudo Y, Miyakawa H (1998) Differential roles of two types of voltage-gated Ca^{2+} channels in the dendrites of rat cerebellar Purkinje neurons. Brain Res 791:43–55.

Williams SR, Stuart GJ (2000) Action potential backpropagation and somato-dendritic distribution of ion channels in thalamocortical neurons. J Neurosci 20:1307–1317.

Williams SR, Tóth TI, Turner JP, Hughes SW, and Crunelli V (1997) The "window" component of the low threshold Ca^{2+} current produces input signal amplification and bistability in cat and rat thalamocortical neurones. J Physiol 505:689–705.

Yasuda R, Nimchinsky EA, Scheuss V, Pologruto TA, Oertner TG, Sabatini BL, Svoboda K (2004) Imaging calcium concentration dynamics in small neuronal compartments. Sci STKE 2004:pl5.

Yingling CD, Skinner JE (1976) Selective regulation of thalamic sensory relay nuclei by nucleus reticularis thalami. Electroencephalogr Clin Neurophysiol 41:476–482.

Yu XJ, Xu XX, He S, He J (2009) Change detection by thalamic reticular neurons. Nat Neurosci 12:1165–1170.

Zhang L, Jones EG (2004) Corticothalamic inhibition in the thalamic reticular nucleus. J Neurophysiol 91:759–766.

Zhou Q, Godwin DW, O'Malley DM, Adams PR (1997) Visualization of calcium influx through channels that shape the burst and tonic firing modes of thalamic relay cells. J Neurophysiol 77:2816–2825.

Zikopoulos B, Barbas H (2006) Prefrontal projections to the thalamic reticular nucleus form a unique circuit for attentional mechanisms. J Neurosci 26:7348–7361.